Nutation versus angular-dependent NQR spectroscopy and impact of underdoping on charge inhomogeneities in YBa$_2$Cu$_3$O$_y$

Rinat Ofer and Amit Keren

Physics Department, Technion-Israel Institute of Technology, Haifa 32000, Israel

We describe two different nuclear quadrupole resonance (NQR) based techniques, designed to measure the local asymmetry of the internal electric field gradient η and the tilt angle α of the main NQR principal axis $\hat{z}$ from the crystallographic axis $\hat{c}$. These techniques use the dependence of the NQR signal on the duration of the radio frequency (rf) pulse and on the direction of the rf field H_1 with respect to the crystal axis. The techniques are applied to oriented powder of YBa$_2$Cu$_3$O$_y$ fully enriched with ^{63}Cu. Measurements were performed at different frequencies, corresponding to different in-plane copper sites with respect to the dopant. Combining the results from both techniques, we conclude that oxygen deficiency in the chain layer lead to a rotation of the NQR main principal axis at the nearby Cu on the CuO$_2$ planes by $\alpha \simeq 20° \pm 5°$. This occurs with no change to η. The axis rotation associated with oxygen deficiency means that there must be electric field inhomogeneities in the CuO$_2$ planes only in the vicinity of the missing oxygen.

I. INTRODUCTION

Hole doping the CuO$_2$ planes of the cuprates creates natural inhomogeneities. Determining the origin and form of these charge inhomogeneities is essential for our understanding of their transport properties. There are several theoretical works suggesting that phase separation is a characteristic of the Hubbard model and therefore an intrinsic property of the CuO$_2$ planes.[1] Moreover, it has been suggested that the phase separation, possibly in the form of strips, can explain many of the unusual properties of the cuprates and leads to the superconductivity (for example, Ref. [2]).

Indeed, some of these materials show phase separation with segregated hole-rich and hole-poor regions. Such inhomogeneities were found in La$_{2-x}$Sr$_x$Cu$_1$O$_4$ by several methods such as nuclear quadrupole resonance (NQR),[3] neutron scattering,[4] and muon spin relaxation (μSR).[5] In addition, scanning tunnel microscope (STM) experiments on underdoped Bi$_2$Sr$_2$CaCu$_2$O$_y$ (Bi-2212) showed local density-of-states modulations[6] and inhomogeneity of the superconducting gap on the samples' surface that can be associated with the distribution of holes in the planes.[7]

In YBa$_2$Cu$_3$O$_y$ (YBCO), phase separation was found at very low doping levels, up to YBCO$_{6.35}$, with neutron scattering from phonons related to charge inhomogeneity.[8] μSR measurements show the existence of a spin-glass phase for a similar doping range.[9] The highest doping in which magnetic order was found in YBCO was in YBCO$_{6.6}$ (Ref. [10]) using neutron scattering. ^{89}Y NMR study in YBCO$_y$ for $y=7$ and 6.6 showed no phase separation at all.[11] Direct detection of charge inhomogeneity in YBCO$_y$ is nearly impossible since STM measurements are very difficult due to oxygen loss in vacuum and surface problems. Various STM experiments in this compound showed an inhomogeneous[12] or relatively homogenous surface,[13] depending on the surface preparation procedure. In these circumstances NQR might be the only tool to probe charge inhomogeneities in YBCO. Moreover, NQR experiments are sensitive to the charge distribution in the bulk and not just on the surface.

In this paper, we present NQR measurements on ^{63}Cu enriched YBCO. This YBCO compound has narrow NQR resonance lines, which allows us to distinguish between different in-plane copper [Cu(2)] and associate each line with a local environment. We then apply two additional NQR based methods called nutation spectroscopy and angle dependent NQR (ADNQR). The two methods are set to measure the quadrupole interaction asymmetry parameter η and the tilt angle α of the NQR main principle axis $\hat{z}$ from the crystal axis $\hat{c}$. This allows us to measure charge inhomogeneity in the CuO$_2$ plane. The main advantage of these techniques is that they can be employed at every frequency in the NQR spectrum. Therefore, unlike NMR, η and α can be determined for each ionic environment separately. Our main conclusion is that for Cu(2) in unit cells with no oxygen deficiency $\alpha \simeq 0$ and $\eta \simeq 0$. However, for every Cu(2) in a unit cell where an oxygen is missing and *only* in these unit cells, $\alpha \simeq 20°$ and $\eta \simeq 0$. Such a tilt of $\hat{z}$ from the crystal axis $\hat{c}$ in special unit cells implies charge inhomogeneities in the CuO$_2$ plane only next to oxygen deficiency.

The paper is organized as follows. In Sec. II we give a general description of NQR and then introduce the less known experimental methods: the nutation spectroscopy and the ADNQR. Theoretical calculations for these techniques are also shown. In Sec. III we describe the experimental setup. The experimental results are presented in Sec. IV. Finally the summary and conclusions on the experimental techniques and their application to YBCO are presented in Sec. V.

II. EXPERIMENTAL TECHNIQUES

A. NQR

In an NQR experiment one uses an rf magnetic pulse in order to cause transitions between the nuclear energy levels. Nuclei with spin $I > 1/2$ can be viewed as positively charged oval objects. As a result, their energy inside a solid depends on their orientation in the electrostatic potential $V(\mathbf{r})$ gener-

ated by the other nuclear and electronic charges. When the nuclear poles are close to positive charges their energy is high and when the poles are close to negative charges the energy is low. The energy difference between different orientations is determined by the electric field gradient (EFG) tensor $V_{ij} = \frac{\partial^2 V}{\partial x_i \partial x_j}$ at the position of the Cu nuclei. The directions can be chosen so that V_{ij} is diagonal. These directions are known as the principal axis of the EFG. Due to Laplace equation ($V_{xx} + V_{yy} + V_{zz} = 0$) the NQR Hamiltonian is determined by only two parameters, ν_q and η, and is given by

$$\mathcal{H}_Q = \frac{\hbar \nu_q}{6} [3I_z^2 - I^2 + \eta(I_x^2 - I_y^2)], \quad (1)$$

where I_α are the nucleus spin operators; ν_q is a frequency scale, determined by the main EFG component V_{zz}, and the quadruple moment of the nucleus Q;

$$\eta = \frac{V_{xx} - V_{yy}}{V_{zz}} \quad (2)$$

is the asymmetry parameter with the convention $|V_{zz}| \geq |V_{yy}| \geq |V_{xx}|$ and therefore $0 \leq \eta \leq 1$.

For the spin 3/2 copper nucleus, the NQR Hamiltonian has two doubly degenerate energy levels, and therefore only one resonance frequency, given by

$$f_{\mathrm{NQR}} = \hbar \nu_q \sqrt{1 + \frac{\eta^2}{3}}. \quad (3)$$

Since ν_q is proportional to V_{zz}, it holds information on the charges surrounding the nucleus. Therefore nuclei sitting in different electronic environments will have different resonance frequencies. η is a parameter that holds information on the anisotropy of the surrounding charges in the x-y plane. In the case of axial symmetry, $\eta = 0$. It is clear from Eq. (3) that in the standard NQR experiment where only the resonance frequency is measured, η and ν_q cannot be separately determined. However, the properties of the rf field turn out to be handy.

The rf pulse Hamiltonian is

$$\mathcal{H}_{\mathrm{rf}} = \gamma \hbar \mathbf{H}_1 \cdot \mathbf{I} \sin \omega t, \quad (4)$$

where, in general, the rf field can be described as

$$\mathbf{H}_1 = H_1 \hat{\mathbf{r}} \quad \hat{\mathbf{r}} = [\sin(\theta)\cos(\phi), \sin(\theta)\sin(\phi), \cos(\theta)], \quad (5)$$

where θ and ϕ the polar angles relating the coil axis to the quadrupolar reference frame.

The signal in the coil after a time t from an on-resonance rf pulse ($\omega = \omega_Q \equiv 2\pi f_{\mathrm{NQR}}$) with a duration t_p is given by[14]

$$I(t_p, t, \theta, \phi, \eta) \propto \lambda(\theta, \phi, \eta)\sin[\lambda(\theta, \phi, \eta)\omega_1 t_p]\sin(\omega_Q t), \quad (6)$$

where $\omega_1 = \gamma H_1$ (γ is the nucleus gyromagnetic ratio) and λ is an angular factor given by

$$\lambda(\theta, \phi, \eta) = \sqrt{r_x^2 a_x^2 + r_y^2 a_y^2 + r_z^2 a_z^2}, \quad (7)$$

where

$$\mathbf{a} = \frac{1}{2\sqrt{3 + \eta^2}}(\eta + 3, \eta - 3, 2\eta). \quad (8)$$

Hence, the signal at time t is a function of both the duration of the rf pulse and the polar angles between the rf direction and the EFG. In the following sections we review two methods that use these parameters to determine η and the angle α between $\hat{\mathbf{z}}$ and $\hat{\mathbf{c}}$.

B. Nutation spectroscopy

The nutation spectroscopy NQR, developed by Harbison *et al.*,[15,16] is a method in which the signals are measured as a function of the duration of the rf excitation pulse t_p. This method is used to determine the asymmetry parameter η. Integrating Eq. (6) over the angles for isotropic powder and Fourier transforming with respect to t_p gives a powder pattern line shape that is described by

$$I(\omega_p, t, \eta) \propto \int_0^{2\pi} d\phi \int_0^\pi \sin \theta d\theta \lambda(\theta, \phi, \eta) \int_{-\infty}^\infty$$
$$\times e^{i\omega_p t_p} dt_p \sin(\lambda(\theta, \phi, \eta)\omega_1 t_p)\sin(\omega_Q t). \quad (9)$$

The Fourier transform part of this integral, over t_p, gives a delta function at the angular frequency,

$$\omega_p(\theta, \phi, \eta) = \lambda(\theta, \phi, \eta)\omega_1. \quad (10)$$

The angular integrals required to complete the calculation of $I(\omega_p, t, \eta)$ demand numerical integration. Nevertheless, the peaks of this function can be obtained by looking at the extremum of $\omega_p(\theta, \phi, \eta)$ with respect to θ and ϕ. This gives three singularities

$$\theta = 0 \quad \omega_{\mathrm{I}} = \frac{2\eta}{2\sqrt{3 + \eta^2}}\omega_1, \quad (11)$$

$$\theta = \pi/2 \quad \phi = 0 \quad \omega_{\mathrm{II}} = \frac{\eta + 3}{2\sqrt{3 + \eta^2}}\omega_1, \quad (12)$$

$$\theta = \pi/2 \quad \phi = \pi/2 \quad \omega_{\mathrm{III}} = \frac{\eta - 3}{2\sqrt{3 + \eta^2}}\omega_1. \quad (13)$$

In the special case of $\eta = 0$ we find $\omega_{\mathrm{II}} = \omega_{\mathrm{III}}$ and $\omega_{\mathrm{I}} = 0$, and therefore there is only one sharp frequency at $0.866\omega_1$. As η grows the three frequencies separate into the three singularities and the pattern broadens. From these singularities η can be extracted by $\eta = (\omega_{\mathrm{III}} - \omega_{\mathrm{II}})/(\omega_{\mathrm{III}} + \omega_{\mathrm{II}})$. Figure 1(a) shows the powder patterns for different values of η for randomly oriented powder.

In the case of an oriented powder, the crystallographic $\hat{\mathbf{c}}$ direction and the EFG $\hat{\mathbf{z}}$ direction are parallel but the crystallographic $\hat{\mathbf{a}}$ (and $\hat{\mathbf{b}}$) directions are random with respect to the EFG $\hat{\mathbf{x}}$ (and $\hat{\mathbf{y}}$) directions. The rf transmission is done perpendicular to $\hat{\mathbf{c}}$ (and $\hat{\mathbf{z}}$). Figure 1(b) shows the nutation line shapes in this case. There is no big difference between powder and oriented powder for $\eta = 0$ but as η grows the difference between the two cases becomes clear.

In general, however, $\hat{\mathbf{z}}$ does not have to be exactly parallel to the $\hat{\mathbf{c}}$ direction of the lattice. This situation is demonstrated
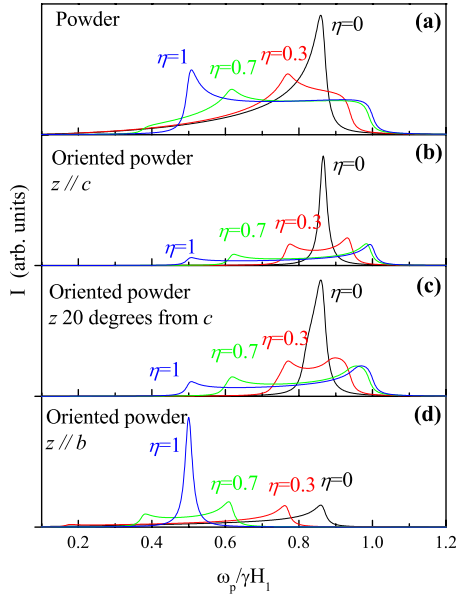
FIG. 1. (Color online) Calculated on-resonance nutation spectra for: (a) powder samples. (b) Perfectly oriented powder where $\hat{z} \| \hat{c}$. (c) Oriented powder where $\hat{z}$ has up to 20° angle from $\hat{c}$ (d) Perfectly oriented powder where $\hat{z} \| \hat{b}$. For the oriented powders the rf transmission is perpendicular to the $\hat{c}$ direction.

in Fig. 2. The angle between $\hat{z}$ and $\hat{c}$ is α. The $\hat{x}$ direction is assumed to be in the a-b plane making an angle φ with $\hat{a}$. Figure 1(c) shows the line shapes when $\alpha = 20°$ and φ is averaged. One can see that with the nutation spectroscopy it is very difficult to distinguish between the case of perfect orientation (panel b) and partial orientation (panel c). Finally,
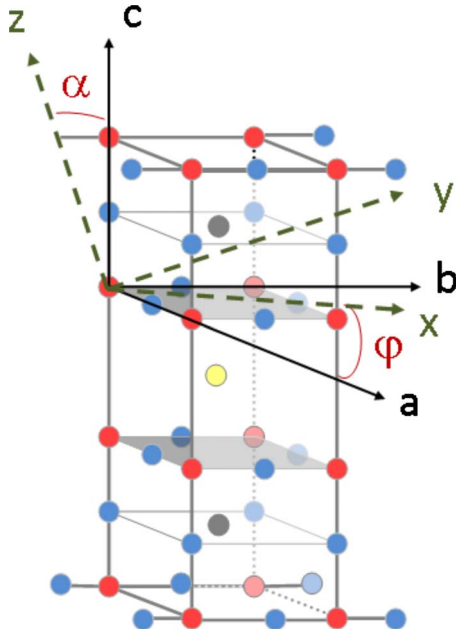

FIG. 2. (Color online) The unit cell of YBCO. An illustration of the rotation of the EFG main principal axis from the crystallographic directions due to the missing oxygen atoms in the chains. The angle between $\hat{z}$ and $\hat{c}$ is α. The $\hat{x}$ direction is in the a-b plane making an angle φ with $\hat{a}$.
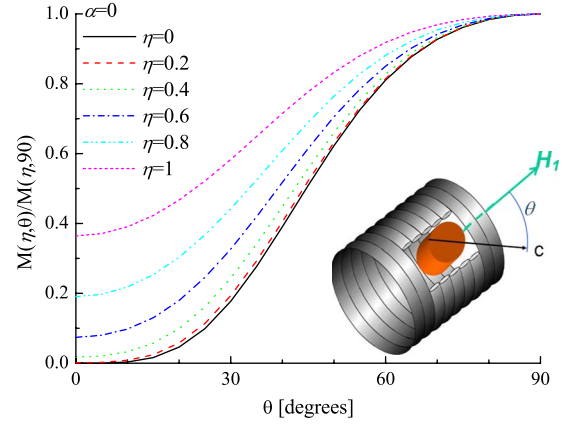

FIG. 3. (Color online) Theoretical echo intensity curves for various values of η calculated from Eq. (15). θ is the polar angle between the rf field and the $\hat{c}$ direction of the lattice in an oriented powder. In this case the $\hat{z}$ direction of the EFG is assumed to be parallel to $\hat{c}$. Inset: basic angle dependent NQR configuration. A sample with a preferred direction is inserted into the coil. The angle θ between them can be varied with a motor.

in Fig. 1(d) we present a case of perfectly oriented powder but with $\hat{z}$ parallel to $\hat{b}$. This case is fundamentally different from previous cases especially when $\eta = 1$.

For a spin-echo sequence, after a time τ from the first pulse there is a refocusing pulse with duration t_r. This adds an additional factor of $\sin^2[\lambda(\theta, \phi, \eta)\omega_1 t_r]$ to the signal. In an NQR experiment, since the spin rotation frequency depends on the orientation of the lattice with respect to the coil, the second pulse cannot perfectly refocus all the magnetization. Harbison *et al.*[16] showed that the additional factor does not change the nutation frequencies $\omega_{I,II,III}$; however, it does change the relative intensities of these frequencies with respect to each other.

The main advantage of the nutation method is that it is relatively simple to execute; it can be carried out on a simple NQR spectrometer without a static magnetic field or additional modifications. This method can also be implemented for powders. It allows the determination of η at every point of the NQR spectrum (unlike NMR, where η can be determined only from the entire spectrum with no local resolution).

C. Angle dependent NQR

The angle dependent NQR technique on an oriented powder was originally developed by Levy and Keren.[17] In this technique the signal intensity for a given frequency is measured as a function of θ, the angle between the direction of the rf field and the crystallographic $\hat{c}$ direction. This technique is sufficient to determine η when the EFG $\hat{z}$ direction is in the crystallographic $\hat{c}$ direction. As we mentioned before this does not have to be the case. In the ADNQR experiment the sample is rotated with respect to the symmetry axis of the coil (see inset of Fig. 3) and the echo intensity is registered for each angle.

From Eqs. (1), (4), and (5) one can see that for $\eta = 0$, $\mathcal{H}_Q$, and $\mathcal{H}_{rf}$ commute when $\theta = 0$. In this case there will be no

spin transitions and no signal. For $\eta > 0$, $\mathcal{H}_Q$, and $\mathcal{H}_{rf}$ do not commute even for $\theta = 0$. In this case we expect a signal even when $\mathbf{H}_1$ is in the $\hat{z}$ direction. In general, Levy and Keren[17] showed that for a $\pi/2$-τ-π pulse sequence, when $\mathbf{H}_1$ is given by Eq. (5), the magnetization in the coil at the time of the echo is given by

$$M(\theta, \phi, \eta) = \frac{\lambda(\theta, \phi, \eta)\hbar\omega_Q}{2K_B T}\sin^3[\lambda(\theta, \phi, \eta)\omega_1 t_{\pi/2}], \quad (14)$$

where $t_{\pi/2}$ is the duration of the $\pi/2$ pulse and $\lambda(\theta, \phi, \eta)$ is the same as in Eq. (7).

In the case of an oriented powder, again with $\hat{z}$ and $\hat{c}$ parallel, and the $\hat{a}$ (and $\hat{b}$) random, M is obtained by averaging over ϕ, namely,

$$M(\eta, \theta) = \frac{1}{2\pi}\int_0^{2\pi}M(\theta, \phi, \eta)d\phi. \quad (15)$$

Theoretical echo intensity curves as a function of θ for various values of η are presented in Fig. 3. A fit of experimental data to these theoretical curves can give the value of η.

Next we discuss the case where $\hat{z}$ has an angle α with $\hat{c}$ as in Fig. 2. In this case $\mathcal{H}_Q$ and $\mathcal{H}_{rf}$ again do not commute even for $\theta = 0$ and we expect a signal even when $\mathbf{H}_1$ is in the $\hat{z}$ direction, for all values of η. To evaluate the signal intensity we can take the unit vector pointing in the direction of $\mathbf{H}_1$ in the crystal coordinate system to be $\hat{r} = \hat{x}\sin\theta + \hat{z}\cos\theta$ and express it as $\hat{r}'$ in the EFG coordinate system using the Euler angles.[18] If we assume, again for simplicity, that $\hat{x}$ is in the a-b plane with an angle φ from $\hat{a}$ as in Fig. 2 then,

$$\hat{r}'(\alpha, \varphi, \theta) = \begin{bmatrix} 1 & 0 & 0 \\ 0 & \cos\alpha & \sin\alpha \\ 0 & -\sin\alpha & \cos\alpha \end{bmatrix}\begin{bmatrix} \cos\varphi & \sin\varphi & 0 \\ -\sin\varphi & \cos\varphi & 0 \\ 0 & 0 & 1 \end{bmatrix}\hat{r}(\theta) \quad (16)$$

and

$$\lambda(\alpha, \varphi, \theta, \eta)$$
$$= \sqrt{\hat{r}_x'^2(\alpha, \varphi, \theta)a_x^2(\eta) + \hat{r}_y'^2(\alpha, \varphi, \theta)a_y^2(\eta) + \hat{r}_z'^2(\alpha, \varphi, \theta)a_z^2(\eta)}. \quad (17)$$

In the case of $\eta = 0$,

$$\lambda(\alpha, \varphi, \theta, \eta = 0)$$
$$= \frac{\sqrt{3}}{2}\sqrt{\cos^2\varphi\sin^2\theta + (\sin\alpha\cos\theta - \cos\alpha\sin\varphi\sin\theta)^2} \quad (18)$$

and the magnetization in the coil as a function of the rotation angle θ is now

$$M(\alpha, \theta, \eta = 0) = \frac{\hbar\omega_Q}{2k_B T}\frac{1}{2\pi}\int_0^{2\pi}\lambda(\alpha, \varphi, \theta, \eta = 0)$$
$$\times\sin^3[\lambda(\alpha, \varphi, \theta, \eta = 0)\omega_1 t_{\pi/2}]d\varphi. \quad (19)$$

Figure 4 shows the magnetization in the coil according to Eq. (19) for different values of alpha.
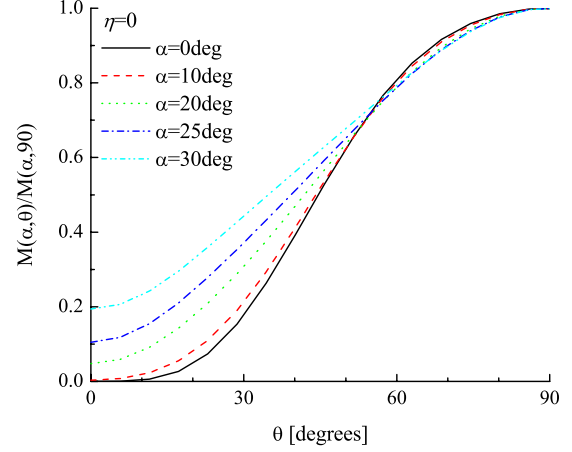

FIG. 4. (Color online) Theoretical echo intensity curves for $\eta = 0$ and various values of α calculated from Eq. (19). θ is the polar angle between the rf field and the c direction of the lattice in an oriented powder.

III. EXPERIMENTAL SETUP

The NQR spectra were obtained using a spectrometer with a homemade automated frequency sweep. The measurements were performed in a coil tunable from 25 to 33 MHz. The data were obtained by applying a spin-echo sequence. Both for the nutation and the ADNQR techniques it is of great importance for the rf field to be homogeneous. For the nutation experiment we measured samples with a small volume inside a long cylindrical coil. The coil's wire goes through a current monitor. This current monitor allows us to perform measurements at different frequencies with the same current through the coil and therefore the same H_1. For the ADNQR we used a spherical coil that gives a more homogenous magnetic field with a better filling factor. The experiment is fully automated, the sample holder is connected to a motor which rotates the sample and can be controlled from the computer.

The measurements were done on YBCO$_y$ oriented powders, with different doping levels. The data were taken at 100 K, which is above T_C for all samples. Previous Cu NQR measurements on YBCO (see Ref. 19) were performed on samples containing both Cu isotopes, Cu^{63} and Cu^{65}, so the frequency lines consisted of doublets of Cu^{63}-Cu^{65}. In this work, for a clearer understanding of the NQR signals, the YBCO samples were all made of enriched copper, meaning that these samples contained only the Cu^{63} isotope. This allows us to distinguish between the different contributions to the NQR line from different local environments.

IV. RESULTS

A. Cu NQR lines of enriched YBCO samples

The frequency sweep lines of YBCO$_y$ samples with different doping at 100 K are presented in Fig. 5. The spectrum is normalized by f^2 in order to correct for population difference and the induced signal in the coil. For the fully doped sample only one resonance is observed. Between $y = 6.85$ and 6.73 two resonances are observed. At $y = 6.68$ there are
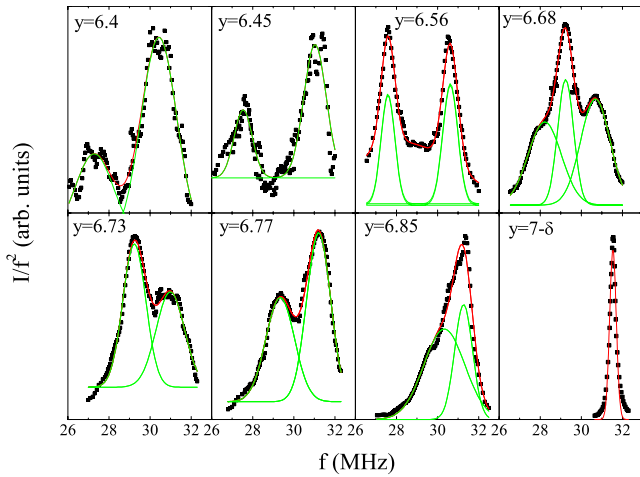
FIG. 5. (Color online) NQR frequency sweep on YBCO$_y$. The solid lines are Gaussian fits performed in order to determine the resonance frequencies.

FIG. 7. (Color online) Schematic illustration of the Cu site in YBCO with locally different oxygen coordinations.

clearly three resonances. The middle one disappears upon further oxygen reduction and below $y=6.45$ again only two resonances are seen. For each sample, the resonance frequencies were extracted from the spectrum. In Fig. 6(a) we plot the oxygen doping as a function of these frequencies. From
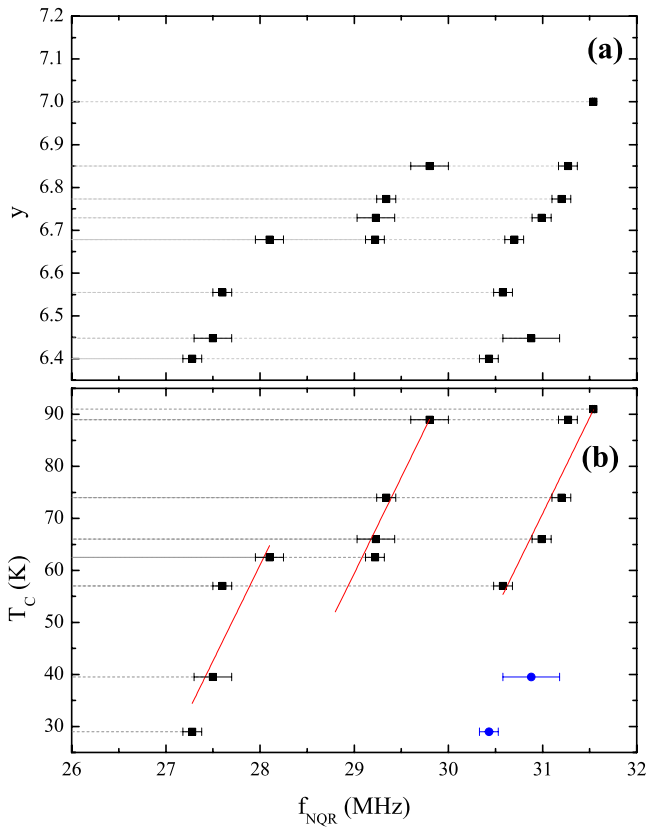

FIG. 6. (Color online) (a) The oxygen doping for different YBCO samples as a function of the NQR frequencies. (b) The superconducting transition temperature of these samples as a function of the NQR frequencies. The blue circular symbols are resonance frequencies coming from the Cu(1) site. The red lines are a fit to three parallel lines, for the three different Cu(2) sites.
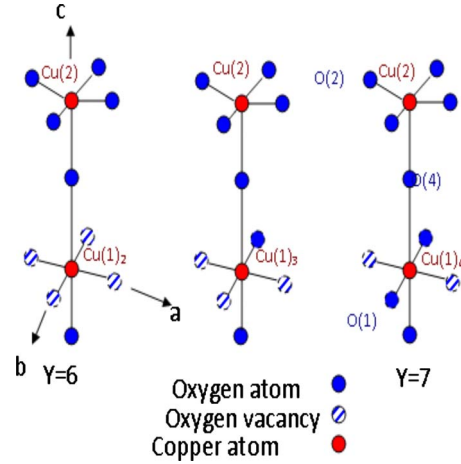
this plot it is clear that there are three different Cu sites.

Earlier NQR measurements done on YBCO$_y$ with both Cu isotopes present, found similar resonance frequencies for similar y values.[19,20] We therefore assign the different resonance frequencies of each sample to different ionic environment, based on these earlier work. For high doping level ($y > 6.5$) all signals come from the plane Cu(2). There are three different types of environment that affect the Cu(2) resonance frequency. They were classified in terms of the number of oxygen surrounding the chain copper Cu(1) neighboring the detected Cu(2). Cu(1)$_4$ stands for a Cu(2) next to a full chain as in YBCO$_7$; in this case the frequency is the highest. Cu(1)$_3$ means Cu(2) whose neighboring Cu(1) is missing one oxygen; the middle frequency belongs to this Cu(2). Finally, Cu(1)$_2$ is when the neighboring chain to the Cu(2) is empty; the lowest frequency belongs to this case. The three possible environments of the Cu(1) are shown schematically in Fig. 7.

It is clear from Fig. 5 that as the doping decreases, the amplitude of the lower frequencies resonances increases at the expense of the high-frequency resonance. This makes sense with our line assignment, as at lower doping there are less Cu(2)$_4$ sites and more Cu(2)$_3$ and Cu(2)$_2$ sites. In addition, at oxygen doping close to 6.5 (i.e., 6.56 and 6.45) the signal from Cu(2)$_3$ is very hard to detect. This is due to the formation of the ortho II phase at these dopings.[21]

In Fig. 6(a) we depict the oxygen level y vs f_{NQR}. Clearly, the more holes are introduced into the planes the more shifted is the frequency. In Fig. 6(b) we plot the superconducting transition temperature T_C as a function of f_{NQR}. For each site, the lower T_C the more shifted are the peaks toward low frequencies. It seems that the rate of change of T_C with f_{NQR}; dT_C/df_{NQR} is identical for all sites as demonstrated by the solid lines. Assuming that the NQR resonance frequency is proportional to the number of charges (which holds in the case where η is constant), this implies that T_C is proportional to the number of free charges in the plane. Since T_C is also proportional to the superfluid density n_s,[22] this means that the rate of conversion of holes to superconducting holes is constant.
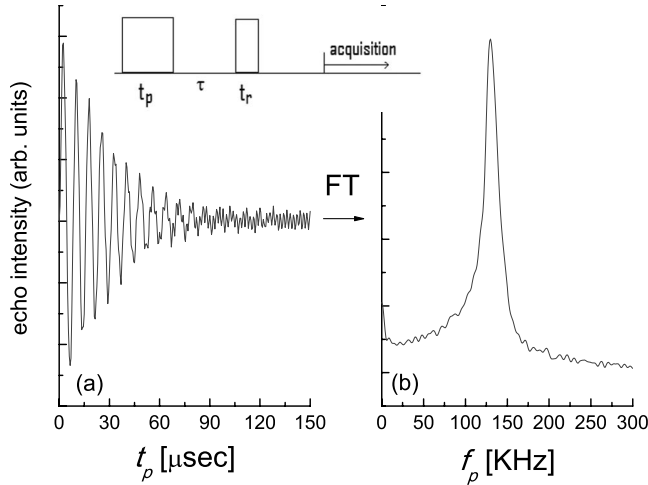
FIG. 8. Inset: the pulse sequence of a nutation experiment. (a) An example of raw data of a nutation experiment for $y=7-\delta$ at 31.5 MHz. The refocusing pulse t_r was 4.4 μs and τ was 32 μs. (b) The data after Fourier transform.

FIG. 9. (Color online) (a) Nutation spectra for YBCO$_{7-\delta}$ with natural abundance of ^{65}Cu and ^{63}Cu. [(b) and (c)] Nutation spectra for YBCO$_{6.73}$ and YBCO$_{6.68}$ enriched with ^{63}Cu. [(d)–(f)] Cu NQR line shape for these three samples, extracted from Fig. 5. The arrows show the frequencies where nutation spectroscopy is applied.

B. Nutation spectroscopy

In the nutation experiment we used a pulse sequence shown in the inset of Fig. 8. The measurement is done by applying this sequence at the resonance frequency of each site, with varying excitation pulse length t_p. The entire echo is integrated and recorded as a function of t_p. An example for raw data for such experiment on a sample with $y=7-\delta$ is shown in Fig. 8(a). The Fourier transform over t_p of this data is presented in Fig. 8(b).

For the Cu(2) of fully doped YBCO it was established[20,23] that the principal component of the EFG is in the $\hat{c}$ direction of the lattice and that $\eta=0$. Looking at Eqs. (10)–(13), in the case of $\eta=0$ there is only one nutation frequency and the ratio ω_p/ω_1 is 0.866. Therefore, from the nutation frequency of the Cu(2) resonance of YBCO$_{7-\delta}$ we can extract ω_1. Since we worked with a constant rf field H_1, we normalized the frequency axis for all samples by ω_1. We then apply this technique to three YBCO$_y$ samples. The results are shown on the left panels of Fig. 9. For each sample the measurements were done at the frequencies marked with arrows on the NQR spectrum, extracted for clarity from Fig. 5, and shown in the right panels.

Figure 9(a) shows the nutation spectrum for YBCO$_{7-\delta}$, measured in both the Cu(2) (31.5 MHz) and the Cu(1) (22 MHz) resonance frequencies. After normalizing the frequency axis by ω_1, as explained above, the Cu(2) has a sharp nutation frequency with $\omega_p/\omega_1=0.866$. However, Cu(1) has a much broader spectrum with $\omega_{pIII}/\omega_1=0.52$ and ω_{pII} which is difficult to determine. The result for the Cu(2) is consistent with $\eta=0$ [see theoretical nutation spectra in Fig. 1(b)]. The result for Cu(1) is consistent with $\eta=0.95\pm0.05$ and $\hat{z}$ pointing in the $\hat{b}$ direction, as shown in Fig. 1(d). These results are in agreement with NMR results on YBCO$_{7-\delta}$ (Refs. 20 and 23) that measured $\eta\simeq0$ for Cu(2) and $\eta\simeq1$ for Cu(1). Similar nutation experiments on powder YBCO$_{7-\delta}$ at room temperature were done by Vega.[24] His results are $\eta=0$ for the Cu(2) and $\eta=0.8$ for the Cu(1).
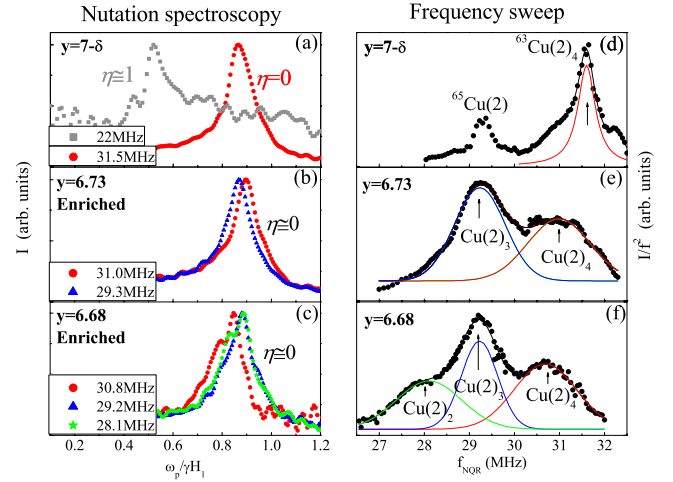
Figures 9(b) and 9(c) show the nutation spectroscopy results for YBCO$_y$ with lower doping levels. For these samples we measured only at the resonance frequencies of the Cu(2). The sample with $y=6.73$ has two resonance lines for two different Cu(2) ionic environments and the sample with $y=6.68$ has three Cu(2) environments. The nutation experiment shows that for these samples, for all three different types of Cu(2) ionic environments, the nutation spectrum is not different from that of the $y=7-\delta$ case, therefore $\eta\simeq0$. This conclusion was verified by using several different H_1 and refocusing pulse time t_r. However, as mentioned in section IIB, the nutation experiment is not sensitive enough to small differences in the orientation of the EFG [see Figs. 1(b) and 1(c)].

C. ADNQR

As mentioned before, in a fully doped YBCO $\hat{z}$ is parallel to the $\hat{c}$ axis of the lattice. Therefore the ADNQR technique can be applied to this sample, using Eq. (15). The result indeed gives $\eta=0$ as was published in Ref. 25 and in agreement with the nutation experiment described above. For lower doping levels however, the exact direction of $\hat{z}$ is unknown. In a previous publication in Ref. 25 we also performed an ADNQR experiment on a YBCO sample with doping of $y=6.68$. Due to lack of information we assumed that $\hat{z}\|\hat{c}$ at all doping. The experimental results from Ref. 25 are shown by the dotted line in Fig. 10(b). Fitting these data to Eq. (15) gave a high value of η in contradiction to the nutation experiment findings in Fig. 9(c) of the present work. The way to settle this contradiction is by allowing $\hat{z}$ to be tilted with an angle α from $\hat{c}$ as in Fig. 2. As mentioned above, in this case the NQR signal does not disappear at $\theta=0$, even in the case of $\eta=0$, as result of $\hat{z}$ EFG component in the a-b plane.

Figures 10(a) and 10(b) show the ADNQR data for the two YBCO samples with doping of $y=7-\delta$ and 6.68. The
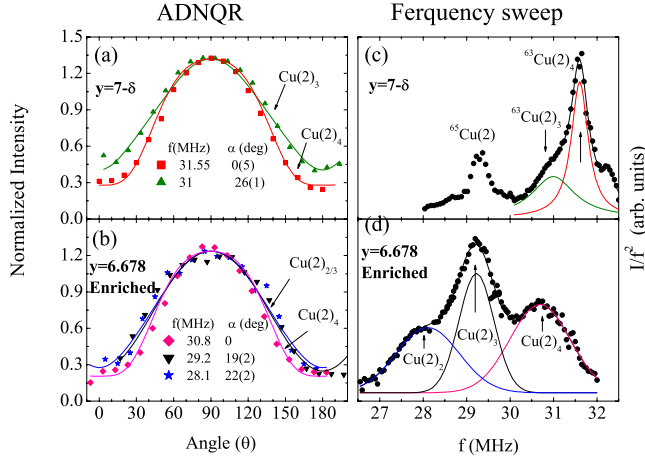
FIG. 10. (Color online) Right panels: Cu NQR line shape for YBCO$_{7-\delta}$ with natural abundance of ^{65}Cu and ^{63}Cu, and for YBCO$_{6.68}$ enriched with ^{63}Cu. The arrows show the frequencies where ADNQR is applied. Left panels: the echo intensity as a function of the angle θ between the rf field and the $\hat{c}$ direction of the lattice for the two samples. The solid lines are fits to Eq. (19).

solid lines are new fits, this time to Eq. (19), namely, $\eta=0$ and tilted principle axis. The fit allows for a finite base line for each sample to account for some unknown amount of misalignment. This misalignment is a result of the nonperfect orientation and some inhomogeneity of the induced field in the coil. These samples' frequency spectrum, taken from Fig. 5, are presented again in Figs. 10(c) and 10(d) for clarity. The arrows in this figure mark the frequencies where AD-NQR was applied.

For the main peak of $y=7-\delta$ the best fit is obtained with $\alpha=0$ and $\eta=0$, as expected. The same result was obtained at the high frequency of the $y=6.68$ sample, which is also associated with Cu(2) in an environment of full chains; Cu(1)$_4$. In contrast, for the other oxygen environments the signal at $\theta \rightarrow 0$ is clearly above the background. Keeping in mined our nutation spectroscopy results, showing that $\eta=0$, this suggests that the value of α is larger than zero. The fit to Eq. (19) gives $\alpha \simeq 20° \pm 5°$. This is the main finding of this work.

V. SUMMARY AND CONCLUSIONS

We used nutation spectroscopy and ADNQR to measure the quadrupole interaction asymmetry parameter η and tilting angle α of the main component of the EFG principal axis $\hat{z}$ from the crystallographic $\hat{c}$ direction. Calculations show that nutation spectroscopy powder patterns for oriented powder are very sensitive to the value of η but they are not very sensitive to α for α up to 20°. In contrast, the ADNQR line shape is sensitive to both η and α. In other words, ADNQR is sensitive to any breaking of the axial symmetry. However,

it is difficult to determine both α and η from ADNQR alone. The combination of the two methods can give a very good estimate on both parameters. We implement these techniques on the in-plane Cu atom of the YBCO compound with different doping levels. We conclude that for both YBCO$_{7-\delta}$ and YBCO$_{6.68}$, η is approximately zero for all Cu(2) resonance frequencies. However, the ADNQR showed that for the underdoped sample there is a clear difference between the Cu(2) neighboring a Cu(1) in a full chain as in a fully doped sample [Cu(1)$_4$] and the Cu(2) neighboring a Cu(1) in an empty or a half filled chain [Cu(1)$_2$-Cu(1)$_3$]. This difference can result from a small change in the EFG principal axis $\hat{z}$ with respect to the lattice directions $\hat{c}$.

The motivation for these experiments was to measure possible charge inhomogeneity or electronic phase separation in the YBCO compound. Both the nutation spectroscopy and the ADNQR for the Cu(2) from a fully oxygenized local environment Cu(1)$_4$, even for lower averaged doping, show a homogeneous charge distribution in the plane. Our combined experiments also imply that only for Cu(2) neighboring a Cu chain with missing oxygen Cu(1)$_2$ or Cu(1)$_3$ is the principle axis $\hat{z}$ of the EFG tensor not along $\hat{c}$, namely, $\alpha \simeq 20° \pm 5°$. Therefore, only from the point of view of a Cu(2) in YBCO$_{6.68}$ neighboring a Cu(1)$_2$ or Cu(1)$_3$, are the $\hat{a}$ and $\hat{b}$ crystallographic directions less identical than in YBCO$_7$. This means that any charge inhomogeneity in the plane is correlated directly with the O dopant atoms and therefore cannot be an intrinsic property of the CuO$_2$ planes alone. It is either generated or pined by missing oxygen.

McElroy et al.[26] came to a similar conclusion by performing spectroscopic imaging scanning tunneling microscopy on Bi-2212 samples. They found strong correlation between the position of localized resonance at -960 meV identified with interstitial oxygen dopants and the size of the local spectral gap. To understand these result, Nunner et al.[27] presented a theoretical model where the dopants modulate the pair interaction locally on an atomic scale. They calculated the correlation between the local density of states and the dopant modulated pair interaction potential. They showed that this model agrees with McElroy's experimental results on Bi-2212. A more recent theoretical work by Mori et al.[28] identified two mechanisms by which the position of the apical oxygen atoms can modulate the pairing interaction within the CuO$_2$ planes.

Our result for the YBCO compound reinforces the surface experiments done on Bi-2212. It shows that the correlation between the electronic spatial variation in the plane and the dopant exists not only in Bi-2212 and it is a property of the bulk and not only of the surface.

[1] U. Low, V. J. Emery, K. Fabricius, and S. A. Kivelson, Phys. Rev. Lett. **72**, 1918 (1994); S. A. Kivelson, I. P. Bindloss, E. Fradkin, V. Oganesyan, J. M. Tranquada, A. Kapitulnik, and C. Howald, Rev. Mod. Phys. **75**, 1201 (2003); M. Capone, G. Sangiovanni, C. Castellani, C. Di Castro, and M. Grilli, Phys. Rev. Lett. **92**, 106401 (2004); M. Aichhorn, E. Arrigoni, M. Potthoff, and W. Hanke, Phys. Rev. B **76**, 224509 (2007); A. Montorsi, J. Stat. Mech.: Theory Exp. (2008), L09001.

[2] E. Arrigoni, E. Fradkin, and S. A. Kivelson, Phys. Rev. B **69**, 214519 (2004).

[3] P. M. Singer, A. W. Hunt, and T. Imai, Phys. Rev. Lett. **88**, 047602 (2002).

[4] K. Yamada, C. H. Lee, K. Kurahashi, J. Wada, S. Wakimoto, S. Ueki, H. Kimura, Y. Endoh, S. Hosoya, G. Shirane, R. J. Birgeneau, M. Greven, M. A. Kastner, and Y. J. Kim, Phys. Rev. B **57**, 6165 (1998).

[5] Ch. Niedermayer, C. Bernhard, T. Blasius, A. Golnik, A. Moodenbaugh, and J. I. Budnick, Phys. Rev. Lett. **80**, 3843 (1998); C. Panagopoulos, J. L. Tallon, B. D. Rainford, T. Xiang, J. R. Cooper, and C. A. Scott, Phys. Rev. B **66**, 064501 (2002).

[6] K. McElroy, R. W. Simmonds, J. E. Hoffman, D.-H. Lee, J. Orenstein, H. Eisaki, S. Uchida, and J. C. Davis, Nature (London) **422**, 592 (2003).

[7] K. M. Lang, V. Madhavan, J. E. Hoffman, E. W. Hudson, H. Eisaki, S. Uchida, and J. C. Davis, Nature (London) **415**, 412 (2002); J. E. Hoffman, K. McElroy, D.-H. Lee, K. M. Lang, H. Eisaki, S. Uchida, and J. C. Davis, Science **297**, 1148 (2002); M. Vershinin, S. Misra, S. Ono, Y. Abe, Yoichi Ando, and Ali Yazdani, *ibid.* **303**, 1995 (2004).

[8] H. A. Mook, Pengcheng Dai, and F. Dogan, Phys. Rev. Lett. **88**, 097004 (2002).

[9] S. Sanna, G. Allodi, G. Concas, A. D. Hillier, and R. De Renzi, Phys. Rev. Lett. **93**, 207001 (2004); R. I. Miller, R. F. Kiefl, J. H. Brewer, F. D. Callaghan, J. E. Sonier, R. Liang, D. A. Bonn, and W. Hardy, Phys. Rev. B **73**, 144509 (2006).

[10] H. A. Mook, Y. Sidis, B. Fauque, V. Baledent, and P. Bourges, Phys. Rev. B **78**, 020506(R) (2008).

[11] J. Bobroff, H. Alloul, S. Ouazi, P. Mendels, A. Mahajan, N. Blanchard, G. Collin, V. Guillen, and J.-F. Marucco, Phys. Rev. Lett. **89**, 157002 (2002).

[12] H. L. Edwards, D. J. Derro, A. L. Barr, J. T. Markert, and A. L. de Lozanne, Phys. Rev. Lett. **75**, 1387 (1995).

[13] N.-C. Yeh, C.-T. Chen, G. Hammerl, J. Mannhart, A. Schmehl, C. W. Schneider, R. R. Schulz, S. Tajima, K. Yoshida, D. Garrigus, and M. Strasik, Phys. Rev. Lett. **87**, 087003 (2001).

[14] J. C. Pratt, P. Raganuthan, and C. A. McDowell, J. Magn. Reson. (1969-1992) **20**, 313 (1975).

[15] G. S. Harbison, A. Solkenbergs, and T. M. Barbara, J. Chem. Phys. **90**, 5292 (1989).

[16] G. S. Harbison and A. Solkenbergs, Z. Naturforsch., A: Phys. Sci. **45**, 575 (1990).

[17] S. Levy and A. Keren, J. Magn. Reson. **167**, 317 (2004).

[18] H. Goldstein, *Classical Mechanics* (Addison-Wesley, Reading, MA, 3rd ed. 2002).

[19] A. J. Vega, W. E. Farneth, E. M. McCarron, and R. K. Bordia, Phys. Rev. B **39**, 2322 (1989); H. Yasuoka, T. Shimiza, Y. Ueda, and K. Kosuge, J. Phys. Soc. Jpn. **57**, 2659 (1988); H. Lutgemeier, Physica C **153**, 95 (1988); Y. Yoshinari, H. Yosuoka, Y. Ueda, K. Koga, and K. Kosuge, J. Phys. Soc. Jpn. **59**, 3698 (1990); M. Takigawa, A. P. Reyes, P. C. Hammel, J. D. Thompson, R. H. Heffner, Z. Fisk, and K. C. Ott, Phys. Rev. B **43**, 247 (1991).

[20] C. H. Pennington, D. J. Durand, D. B. Zax, C. P. Slichter, J. P. Rice, and D. M. Ginsberg, Phys. Rev. B **37**, 7944 (1988).

[21] H. Lutgemeier, S. Schmenn, P. Meuffels, O. Storz, R. Schollhorn, Ch. Niedermayer, I. Heinmaa, and Yu. Baikov, Physica C **267**, 191 (1996).

[22] R. Ofer, G. Bazalitsky, A. Kanigel, A. Keren, A. Auerbach, J. S. Lord, and A. Amato, Phys. Rev. B **74**, 220508(R) (2006).

[23] T. Shimizu, Hiroshi Yasuoka, Takashi Imai, Toshinobu Tsuda, Toshiro Takabatake Yasuhiro Nakazawa, and Masayasu Ishikawa, J. Phys. Soc. Jpn. **57**, 2494 (1988).

[24] A. J. Vega, Isr. J. Chem. **32**, 195 (1992).

[25] R. Ofer, S. Levy, A. Kanigel, and A. Keren, Phys. Rev. B **73**, 012503 (2006).

[26] K. McElroy, J. Lee, J. A. Slezak, D.-H. Lee, H. Eisaki, S. Uchida, and J. C. Davis, Science **309**, 1048 (2005).

[27] T. S. Nunner, P. J. Hirschfeld, B. M. Andersen, A. Melikyan, and K. McElroy, Physica C, **460-462**, 446 (2007).

[28] M. Mori, G. Khaliullin, T. Tohyama, and S. Maekawa, Phys. Rev. Lett. **101**, 247003 (2008).